

The effect of finite-range interactions in classical transport theory

Sen Cheng and Scott Pratt
Department of Physics and National Superconducting Cyclotron Laboratory
Michigan State University
East Lansing Michigan, 48824

Peter Csizmadia
RMKI Research Institute for Particle and Nuclear Physics
P.O. Box 49, Budapest, 1525, Hungary

Yasushi Nara
Riken BNL Research Center, Brookhaven National Laboratory, Upton, NY 11973

Dénes Molnár and Miklos Gyulassy
Department of Physics, Columbia University
538 120th St., New York, NY 10027

Stephen E. Vance
Physics Department, Brookhaven National Laboratory, Upton, NY 11973

Bin Zhang
Department of Chemistry and Physics, Arkansas State University
P.O. Box 419, State University, Arkansas 72467-0419
(April 26, 2024)

The effect of scattering with non-zero impact parameters between constituents in relativistic heavy ion collisions is investigated. In solving the relativistic Boltzmann equation, the characteristic range of the collision kernel is varied from approximately one fm to zero while leaving the mean-free path unchanged. Modifying this range is shown to significantly affect spectra and flow observables. The finite range is shown to provide effective viscosities, shear, bulk viscosity and heat conductivity, with the viscous coefficients being proportional to the square of the interaction range.

I. INTRODUCTION

A principal goal of relativistic heavy ion collisions is to experimentally discern bulk properties of the excited vacuum. To accomplish this aim it is imperative that one understands the implications of the finite size and lifetime of the global reaction. Two microscopic length scales govern the importance of finite-size effects, the mean free path and the range of interaction. Microscopic models, e.g., those based on the Boltzmann equation, easily incorporate the effects of a finite mean free path. Such effects can be linked to viscous terms in analogous hydrodynamic descriptions.

In intermediate-energy collisions, where excitation energies are tens of MeV per nucleon, the role of the finite range to the strong interaction has been studied in its relation to the surface energy of nuclear matter. In such Boltzmann descriptions the binding energy of nuclear matter is introduced via the mean field, with the coarseness of the mean field mesh being adjusted so that the effect of the interaction range is effectively tuned to reproduce the surface energy of nuclear matter. In non-relativistic molecular dynamics, the effects of hard-sphere interactions have also been investigated. In this case the size of the spheres represents a length scale which can strongly affect bulk properties of the matter at high density. However, in the context of a Boltzmann description, where n -body correlations are explicitly neglected, the effects of a finite range inherent to the scattering kernel have not been analyzed for their impact on final-state observables.

It is the goal of this study to ascertain the importance of this second length scale in high-energy collisions. By varying the interaction range in the scattering kernel, while leaving the mean free path unchanged, we study the manifestations of a non-zero interaction range. We demonstrate that a finite interaction range contributes to viscous terms in a manner similar to the finite mean free path, but with different dependencies with respect to density and temperature. We find that the finite range of the interaction affects the evolution of heavy-ion reactions, and alters final-state observables, especially the elliptic flow.

In the next section we present a formal review of the Boltzmann equation and show how viscosities arise from the interaction range. In section III we show how spectra and flow observables are sensitive to the finite range. We discuss algorithmic sensitivities which cannot be ignored when the interaction range is non-zero, and compare results

compiled from four similar numerical implementations of the Boltzmann equation to illustrate this sensitivity. We show how viscous heating can be understood from analyzing the collision kernel in Sec. IV. In particular we present a comparison of heating derived from analysis of the collision kernel with the heating observed in a simple simulation. A discussion of the importance of non-local interactions and the associated causality problems is provided in the summary.

II. CONNECTING VISCOSITIES TO FINITE-RANGE INTERACTIONS

A. The Role of the Collision Kernel in Boltzmann Descriptions

The Boltzmann equation can be expressed,

$$\frac{\partial}{\partial t} f(\mathbf{p}, \mathbf{r}, t) + \mathbf{v}_p \cdot \nabla f(\mathbf{p}, \mathbf{r}, t) + \mathbf{F}(\mathbf{r}, t) \cdot \nabla_p f(\mathbf{p}, \mathbf{r}, t) = \int d^3 q d^3 q' d^3 p' d^3 r' dt' \quad (1)$$

$$\cdot \{f(\mathbf{q}, \mathbf{r}, t) f(\mathbf{q}', \mathbf{r}', t') K(\mathbf{r} - \mathbf{r}', t - t'; \mathbf{q}, \mathbf{q}'; \mathbf{p}, \mathbf{p}') - f(\mathbf{p}, \mathbf{r}, t) f(\mathbf{p}', \mathbf{r}', t') K(\mathbf{r} - \mathbf{r}', t - t'; \mathbf{p}, \mathbf{p}'; \mathbf{q}, \mathbf{q}')\}, \quad (2)$$

where f is the phase space density and \mathbf{F} is the force $d\mathbf{p}/dt$ felt by a particle at position \mathbf{r} . The collision kernel $K(\mathbf{r} - \mathbf{r}', t - t'; \mathbf{q}, \mathbf{q}'; \mathbf{p}, \mathbf{p}')$ describes the differential probability for scattering a pair of particles separated in space-time by $x - x'$ with initial momenta \mathbf{q} and \mathbf{q}' into final states with momenta \mathbf{p} and \mathbf{p}' . The range of the collision kernel in coordinate space is the subject of this paper.

Integrating over the collision kernel should yield the cross section,

$$\int d^3 r' dt' K(\mathbf{r} - \mathbf{r}', t - t'; \mathbf{q}, \mathbf{q}'; \mathbf{p}, \mathbf{p}') = \frac{1}{(2\pi)^3} \frac{d\sigma}{d^3 p_{\text{rel}}} v_{\text{rel}} \delta^3(\mathbf{p} + \mathbf{p}' - \mathbf{q} - \mathbf{q}'), \quad (3)$$

where \mathbf{p}_{rel} is the relative momentum of the outgoing pair $(\mathbf{p} - \mathbf{p}')/2$. By inspection of Eq. (3), one can see that the coordinate-space dependence of K appears rather arbitrary as long as it integrates to the free-space cross section. Indeed, results at low density, where particles interact only pairwise, are unaffected by the form of K as long as the range is much less than the mean free path and much less than the characteristic dimensions of the reaction volume.

Any non-zero extent of the collision kernel leads to problems with super-luminal transport. However, these problems are easily defeated by restricting the kernel to being local, i.e.,

$$K(\mathbf{r} - \mathbf{r}', t - t'; \mathbf{q}, \mathbf{q}'; \mathbf{p}, \mathbf{p}') = \frac{1}{(2\pi)^3} \delta^3(\mathbf{r} - \mathbf{r}') \delta(t - t') \cdot \frac{d\sigma}{d^3 \mathbf{p}_{\text{rel}}} v_{\text{rel}} \delta^3(\mathbf{p} + \mathbf{p}' - \mathbf{q} - \mathbf{q}'). \quad (4)$$

The Boltzmann equation can now be written in a manifestly covariant form.

$$\left(u_{\mathbf{p}}^{\mu} \partial_{\mu} + F^{\mu} \frac{\partial}{\partial p^{\mu}} \right) f(\mathbf{p}, \mathbf{r}, t) = \frac{1}{(2\pi)^3} \int \frac{d^3 q'}{E_{q'}} \frac{d^3 q}{E_q} \cdot \left\{ \sqrt{(q \cdot q')^2 - m^4} \frac{d\sigma}{d^3 \tilde{\mathbf{p}}_{\text{rel}}} f(\mathbf{q}, \mathbf{r}, t) f(\mathbf{q}', \mathbf{r}, t) \right. \quad (5)$$

$$\left. - \sqrt{(p \cdot p')^2 - m^4} \frac{d\sigma}{d^3 \tilde{\mathbf{q}}_{\text{rel}}} f(\mathbf{p}, \mathbf{r}, t) f(\mathbf{p}', \mathbf{r}, t) \right\}$$

Here, $u_{\mathbf{p}}$ is the four-velocity of a particle with momentum \mathbf{p} , F^{μ} is the force $dp^{\mu}/d\tau$, and $\tilde{\mathbf{p}}_{\text{rel}}$ is the relative momentum of the outgoing particles in the center of mass.

B. Effective Viscosities from Finite-Range Interactions

In this section we describe how interaction over a finite range contributes to the shear viscosity, η , the bulk viscosity, ζ , and the thermal conductivity, χ . We relate the range of the interaction to all three coefficients. In order to make this connection, we consider two particles which scatter from one another, separated by a distance $\mathbf{r} = \mathbf{r}_2 - \mathbf{r}_1$. Combining this finite separation with the velocity gradient, one sees that the first particle interacts with particles which have a higher average energy. By evaluating the rate at which energy is transferred to the first particle from colliding with more energetic particles, we find an expression for the rate at which heat is deposited to the region defined by \mathbf{r}_1 . By comparing to analogous expressions from hydrodynamics, we derive expressions for all three viscous terms in terms of the interaction range, $r = |\mathbf{r}_1 - \mathbf{r}_2|$, the density n , and the collision rate Γ .

Choosing a reference frame such that the velocity of bulk matter at the location of the first particle is zero, the collective velocity at \mathbf{r}_2 is

$$v_i = A_{ij}r_j, \quad A_{ij} = \frac{\partial v_i}{\partial r_j}. \quad (6)$$

For an elastic collision where two particles of identical mass simultaneously change their momenta, the radial components of the momenta must be interchanged by the collision if energy, linear momentum and angular momentum are to be conserved. Physically, this corresponds to the scattering from the interior or exterior surface of a hard sphere. The average energy change of the first particle is then

$$\langle \delta E_1 \rangle = \langle E_{2,r} \rangle - \langle E_{1,r} \rangle = \frac{m}{2} \langle (\mathbf{v} \cdot \hat{r})^2 \rangle. \quad (7)$$

The mass term m is not to be taken literally as the mass of the particles, since the averaging may include factors of the velocity to account for the flux or it may have a complicated form to accommodate a desired differential cross section. For relativistic motion, the mass might incorporate the lateral motion of the particles. Writing $\langle \delta E_1 \rangle$ in terms of A ,

$$\langle \delta E_1 \rangle = \frac{m}{2r^2} \langle (r_i A_{ij} r_j)^2 \rangle. \quad (8)$$

One can perform the average over the directions of \mathbf{r} using the identity,

$$A_{ij} A_{kl} \langle r_i r_j r_k r_l \rangle = A_{ij} A_{kl} \frac{r^4}{15} (\delta_{ij} \delta_{kl} + \delta_{ik} \delta_{jl} + \delta_{il} \delta_{jk}). \quad (9)$$

One can then express $\langle \delta E_1 \rangle$ in terms of A and r .

$$\begin{aligned} \langle \delta E_1 \rangle &= \frac{mr^2}{30} \left((\text{Tr}A)^2 + \frac{1}{2} \sum_{ij} (A_{ij} + A_{ji})^2 \right) \\ &= \frac{mr^2}{30} \left[(\nabla \cdot v)^2 + \frac{1}{2} \sum_{ij} \left(\frac{\partial v_i}{\partial r_j} + \frac{\partial v_j}{\partial r_i} \right)^2 \right]. \end{aligned} \quad (10)$$

The rate at which the entropy increases due to these interactions is given by the density multiplied by the rate at which collisions deposit energy non-locally,

$$\begin{aligned} \partial \cdot S &= \frac{n\Gamma}{T} \langle \delta E_1 \rangle \\ &= \frac{n\Gamma mr^2}{30T} \left[(\nabla \cdot v)^2 + \frac{1}{2} \sum_{ij} \left(\frac{\partial v_i}{\partial r_j} + \frac{\partial v_j}{\partial r_i} \right)^2 \right]. \end{aligned} \quad (11)$$

Here, Γ is the collision rate experienced by a single particle and n is the density.

It is notable that only the symmetric part of A contributes to $\langle \delta E_1 \rangle$. This owes itself to conservation of angular momentum which forbids rotational motion from being transferred between particles. In fact, if one had derived an expression for $\langle \delta E_1 \rangle$ using v^2 instead of v_r^2 , the resulting expression would have included the odd parts of A which would correspond to rotational motion, $\nabla \times \mathbf{v}$. These terms would have no hydrodynamical analog as they would have reflected a violation of angular momentum conservation.

We now provide analogous expressions for Eq. (11) in the language of hydrodynamics. The expression for entropy production [1] in terms of velocity gradients is

$$\partial \cdot S = \frac{\eta}{2T} \sum_{ij} \left(\frac{\partial v_i}{\partial x_j} + \frac{\partial v_j}{\partial x_i} - \frac{2}{3} \delta_{ij} \nabla \cdot \mathbf{v} \right)^2 + \frac{\zeta}{T} (\nabla \cdot \mathbf{v})^2 + \frac{\chi}{T^2} (\nabla T)^2. \quad (12)$$

One can extract the coefficients by comparing Eq. (11) to the first two terms in Eq. (12).

$$\eta = \frac{mn\Gamma r^2}{30} \quad (13)$$

$$\zeta = \frac{mn\Gamma r^2}{18}. \quad (14)$$

Applying similar reasoning, one can also derive an expression for the thermal conductivity. First, we relate the temperature gradient to the energy flow. Again, we consider particles separated by \mathbf{r} . If collisions occur between two particles at locations with different temperatures, the average energy exchanged is

$$\delta E_1 = \frac{1}{2} C_r \mathbf{r} \cdot \nabla T. \quad (15)$$

Here C_r represents the change in radial kinetic energy per particle per change in temperature,

$$C_r = \frac{\partial}{\partial T} E_r. \quad (16)$$

In the non-relativistic limit, $C_r = 1/2$.

Since the exchange corresponds to moving an energy a finite distance over an effective time given by the collision rate, one can define the average momentum density in terms of the energy flow.

$$M_i = -\frac{n\Gamma C_r}{4} \langle r_i r_j \rangle \frac{\partial T}{\partial x_j}. \quad (17)$$

$$\mathbf{M} = -\frac{n\Gamma C_r r^2}{12} \nabla T \quad (18)$$

An extra factor of 1/2 was added to correct for double counting the collisions.

One can relate the energy flow to the entropy production,

$$\frac{dS}{dt} = \int d^3x \frac{1}{T} \frac{\partial \epsilon}{\partial t} \quad (19)$$

$$= - \int d^3x \frac{1}{T} \nabla \cdot \mathbf{M} \quad (20)$$

$$= \int d^3x \frac{n\Gamma C_r r^2}{12T^2} (\nabla T)^2, \quad (21)$$

where the continuity equation has been applied. One can now compare to the last term in Eq. (12) to obtain the thermal conductivity χ .

$$\chi = \frac{n\Gamma C_r r^2}{12}. \quad (22)$$

The forms for the three coefficients, η , ζ and χ , fundamentally differ from the forms that result from considering a non-zero mean free path ℓ . The viscous coefficients that result from finite ℓ are independent of density and scale inversely with the cross section [1]. The coefficients arising from a non-zero interaction range r scale as the square of the density and are proportional to the cross section. Thus, non-local interactions provide viscosities that are important in wholly different conditions than those where the finite mean free path plays an important role. For a rapidly expanding system, finite-range interactions play an important role when the interaction range multiplied by the velocity gradient provides velocities of similar magnitudes to local thermal velocities. Such conditions exist in the first one fm/c of highly relativistic hadronic collisions.

The expressions here derive from a very specific picture, non-relativistic particles moving on straight-line trajectories punctuated by sharp collisions when the separation equals r . However, all interaction at a finite distance should result in viscous behavior. Relating the distance r to the cross section might involve a detailed microscopic evaluation of the collision kernel. This is especially true for relativistic motion. Despite the complications, one indeed expects the distance r^2 to be of similar magnitude to collision cross sections. It would be interesting to discern whether the ratio between the shear and bulk viscosities varies for different scattering models.

III. SPECTRA AND FLOW

A. Sampling Factors and Scattering Algorithms

Numerical realization of the Boltzmann equation is usually accomplished by performing a classical simulation of the event and applying a large over-sampling factor λ [2,3]. For instance, if one is sampling a system with 100 particles the Boltzmann simulation might simulate the trajectories of 3200 particles which would correspond to $\lambda = 32$. The scattering kernel must be diminished by a factor of $1/\lambda$ to ensure that the scattering rate and mean free path is independent of λ . As the Boltzmann equation is built on the hypothesis that the evolution is completely described by the one-body distribution, the Boltzmann limit is realized for large λ as the correlations between particles becomes negligible.

The most common way in which the scattering rates are scaled by $1/\lambda$ is through reducing the cross section. Usually, particles that pass within a distance $\sqrt{\sigma/\pi}$ of one another are scattered. Scaling the cross section by a factor of $1/\lambda$ leaves the collision rate and mean free path unchanged, and in the limit of large λ leads to a purely local scattering kernel which solves numerous problems associated with non-causal transmission of information and invariance to Lorentz boosts.

Although one can solve the covariance problems by choosing a large λ , one must then understand whether ignoring the finite interaction range has affected the results. More realistically, particles do interact at a finite range through mutually coupling to classical fields or through the quantum exchange of particles. A variety of ideas have been discussed in the literature for including such interactions in ways which preserve covariance and are consistent with the uncertainty principle [4]. However, due to an assortment of technical challenges, all such approaches remain in the development stage. Since most comparisons with experiment continue to be performed with Boltzmann approaches and since understanding the effect of finite interaction will be more clear with a simple model, we begin our study of finite-range effects by analyzing classical Boltzmann treatments.

For the investigations described in this subsection, we will always associate large sampling factors with a reduction in the effective range of the interaction. However, that is not necessarily the case. Instead of reducing the spatial extent of the cross section, one could reduce the probability of scattering by a factor of $1/\lambda$, i.e. not all particles passing within a distance $\sqrt{\sigma/\pi}$ of one another would scatter. For high sampling rates collision-finding meshes with granularities determined by the interaction range are necessary for efficient numerical algorithms. By reducing the cross section, instead of reducing the scattering probability, one is able to reduce the mesh size which results in significantly faster execution.

As mentioned above, particles typically scatter in Boltzmann algorithms when they pass within $\sqrt{\sigma/\pi}$ of one another, at a time chosen to correspond to the point of closest approach. Aside from choosing the range of the collision kernel, many other aspects of such algorithms are arbitrary. For instance, one might expect that particles should scatter with an impact-parameter-dependent probability that has a more complicated form than a simple step function. Even in the non-relativistic limit, scattering at the point of closest approach violates conservation of angular momentum. In some algorithms the reaction plane is preserved in each scattering which has been shown to affect resulting flows in the cascade limit ($\lambda = 1$) [5]. Finally, scatterings need not occur instantly. By delaying the particles a certain time before they emerge with their asymptotic momenta, one can effectively alter the pressure. One must coordinate the time delays with in-medium modifications and knowledge of the phase shifts in order to be ergodically consistent with thermodynamic properties at the level of the second virial coefficient [6].

In the cascade limit, all scattering algorithms carry a degree of arbitrariness due to issues involving Lorentz invariance [7,8]. One problem deals with the ordering of collisions in time. Each collision can be assigned a point in space time. Since many points would have space-like separations, time ordering is frame dependent. Finally, since each collision involves changing trajectories over a finite separation (when $\lambda \neq \infty$) the final outcome can be affected by the time-ordering prescription.

A second aspect of arbitrariness deriving from relativistic considerations derives with what is meant by ‘‘point of closest approach’’. Since altering the two trajectories simultaneously is inherently frame dependent one must choose a prescription for the time at which each particle is to change course due to the collision. To illustrate this we consider two particles with momenta p_1 and p_2 at space-time coordinates x_1 and x_2 . One can solve for the points on their trajectories, x'_1 and x'_2 , where they would reach the point of closest approach as measured by an observer in the two-particle center-of-mass, by solving for the point where the relative separation becomes perpendicular to the relative momentum,

$$x'^{\mu}_1 = x^{\mu}_1 + p^{\mu}_1 \frac{P \cdot (X - x_1)}{p_1 \cdot P} \quad (23)$$

$$x_2'^{\mu} = x_1^{\mu} + p_2^{\mu} \frac{P \cdot (X - x_2)}{p_2 \cdot P} \quad (24)$$

$$0 = (x_1' - x_2') \cdot (q - P \frac{P \cdot q}{P^2}). \quad (25)$$

Here P and q are the total and relative momenta respectively, and $P \cdot X/\sqrt{s}$ is the time at which the collision occurs as measured by an observer in the center-of-mass frame. One can solve Eq.s (23-25) for $P \cdot X$, then inserting into Eq.s (23) and (24) one can solve for x_1' and x_2' .

An algorithmic choice that would retain covariance at the two-body level would be to alter the two momenta at x_1' and x_2' even though the times would not be simultaneous in other frames. However, in a dense medium particles may be involved in several collisions which may result in a variety of events being scheduled between the times t_1' and t_2' . In fact, a particle might be assigned a collision time that precedes its creation. Additionally, Boltzmann algorithms often incorporate collision-finding or mean-field meshes. Prescriptions where the two scattered particles have their trajectories altered at different times become problematic when coordinating the evolution with the mesh. The most common algorithmic choice involves choosing a fixed frame to define collision times, then altering the trajectories at the point of closest approach as measured in that frame. This prescription becomes questionable when collective velocities become relativistic. Such is the case at RHIC where particle emission is spread over 10 units of rapidity. This problem can be somewhat alleviated by ordering the collisions according to $\tau = (t^2 - z^2)^{1/2}$. This choice seems reasonable for ultra-relativistic collisions where conditions are determined largely by τ , but seems unreasonable for lower energy collisions where longitudinal boost invariance is not realized.

B. Comparing Results from Four Algorithms

To illustrate the sensitivity of results to algorithmic choices, we compare results from four numerical approximations to the Boltzmann equation which are realized in four separate models, each arising from a different author. All the algorithms discussed here scatter particles instantaneously at the point of closest approach, and all the models assume a simple s -wave form to the cross section. Each algorithm was executed from the same initial conditions, and each was executed both in the cascade limit ($\lambda = 1$) and with a high sampling factor, $\lambda = 16$. Due to the arbitrariness inherent to algorithms with finite-range interactions it should not be surprising for results to vary between codes with $\lambda = 1$, but it is expected that results from the four approaches should be indistinguishable in the large λ limit.

The four models differ in their definition of “simultaneous”, in their time-ordering prescriptions and in whether they preserve the scattering plane in two-particle scattering. The four algorithms compared here represent the following choices:

1. ZPC: A parton cascade code authored by B. Zhang [9]. Particles scatter at the point of closest approach, simultaneous in a fixed reference frame. This time is determined by first finding the space-time points x_1' and x_2' , where the two particles would scatter should they alter their trajectories simultaneously in the two-particle center-of-mass frame. In a designated laboratory frame, a time is determined by averaging t_1' and t_2' . The trajectories of both particles are simultaneously altered at this average time. The reaction plane is preserved in each two-body scattering, and rescattering between the same partners is allowed after one particle has rescattered.
2. GROMIT- t : A generic scattering engine developed for the RHIC Transport Theory Collaboration (RTTC) [10]. This should be identical to ZPC.
3. MPC(0.4.0): A Boltzmann description authored by D. Molnár [11]. The principal difference with the codes above is that the reaction plane is not preserved in the two-body scattering. Another difference is that rescattering between collision partners is not allowed until both particles have rescattered. It should be noted that MPC has switches which make it possible to reproduce the choices described in ZPC and GROMIT- t .
4. GROMIT- τ : Another version of cascade/Boltzmann engine developed by the RTTC collaboration with collisions ordered by τ to be appropriate for ultra-relativistic collisions [10]. The space-time points at which the two particles would scatter had the particles scattered simultaneously in the two-particle rest frame, x_1' and x_2' , are used to generate two proper times, τ_1' and τ_2' . The average $\tau' = (\tau_1' + \tau_2')/2$ is then used for ordering. Both trajectories are altered when their proper time equals τ' . The reaction plane is preserved in the scattering and scattering between the same pair of particles is allowed after one of the particles has rescattered.

Calculations were performed for all four models with identical initial conditions based on a thermal Bjorken geometry [12]. In Bjorken coordinates, the time is replaced by a proper time,

$$\tau \equiv \sqrt{t^2 - z^2}, \quad (26)$$

and the position along the beam axis, z , is replaced by the effective coordinate,

$$\eta \equiv \frac{1}{2} \log \left(\frac{t+x}{t-z} \right). \quad (27)$$

The coordinate η also gives the rapidity of an observer moving at constant velocity from the origin at $t = 0$ to the space-time point (t, z) .

Thermal emission from a Bjorken geometry would be realized by choosing thermal sources with positions equally distributed in η , with source rapidities $y_s = \eta$, and with emission taking place at a fixed proper time, τ . Such emission would appear invariant to boosts along the beam axis. In the calculations described here, the sources are confined to a finite range in η ,

$$-2 < \eta < 2. \quad (28)$$

The transverse spatial coordinates were randomly placed in a cylinder of radius 5 fm. The simulation involved 2400 pions and 240 protons which were assigned momenta according to a thermal distribution with a temperature $T = 180$ MeV for the protons and $T = 165$ MeV for the pions, to roughly achieve consistency with spectra resulting from heavy ion collisions. The initial particle densities were 7.64 pions and 0.764 protons per fm³. To be as simple as possible, constant cross sections were imposed independent of the species involved.

The resulting spectra at mid-rapidity as calculated with GROMIT- τ are shown in Fig. 1 for four different cross sections, 0, 10, 20 and 40 mb. These calculations were performed with a sampling factor $\lambda = 32$. For larger cross sections, the pion spectra are cooler while the proton spectra are somewhat hotter. The difference would be more pronounced had the pion and proton distributions been initialized with identical temperatures.

Figure 2 displays spectra from GROMIT- τ with $\sigma = 40$ mb for four different sampling factors, $\lambda = 1, 2, 8$ and 32. The sensitivity to λ is remarkable. For small λ it appears that both the pion and proton spectra become hotter. Results appear to converge for $\lambda \rightarrow \infty$ as the $\lambda = 8$ and $\lambda = 32$ results are barely distinguishable. In all the models investigated here, the final-state transverse energies were higher for small sampling factors. We attribute this reduction in cooling to viscous effects arising from finite-range interactions.

In the upper panel of Fig. 3 the resulting spectra from the four algorithms are displayed in the cascade limit. The slopes vary by approximately 20 MeV. The same results are displayed in the lower panel of Fig. 3 but with a high sampling factor, $\lambda = 16$. The various algorithms are then in agreement. Since the hadrons are initially separated by approximately 1/3 fm, while the interaction range is 1.1 fm, it is not surprising that the $\lambda = 1$ result is sensitive to the scattering algorithm.

For each algorithm the spectra fall significantly more steeply when produced with a higher sampling factor λ . This is especially true for the proton spectra, which suggests that radial flow might be stronger in the cascade limit. Since the average transverse energy for pions is also larger in the cascade limit, one can infer that longitudinal cooling is significantly suppressed through particles interacting at a finite range.

C. Elliptic Flow

As a second exploration of the sensitivities to the sampling factor, we consider elliptic flow as observed from the GROMIT- τ algorithm. In this case cyclic boundary conditions in η were employed to simulate a truly boost-invariant system. The densities of protons and pions were chosen identically as above, $n_\pi = 7.64$ fm⁻³, $n_p = 0.764$ fm⁻³ at $\tau = 1.0$ fm/c. The temperatures for the pions and protons were again chosen to be 165 MeV and 180 MeV respectively. Aside from the cyclic boundary conditions in η the only difference with the initial conditions used in the previous subsection is that the particles were confined to an ellipse rather than a circle in the transverse direction. The two radii of the ellipse were 5 fm and 2.5 fm.

The elliptical shape resulted in elliptic flow which is parameterized by the observable v_2 .

$$v_2 = \langle \cos(\phi - \phi_0) \rangle, \quad (29)$$

where ϕ_0 specifies the direction of the reaction plane which contains the short axis of the ellipse. Elliptic flow has been proposed as a means for determining the equation of state of the matter at early times [14–20].

Resulting flows are shown in Fig. 4 and Fig. 5 for two cross sections, 10 mb and 40 mb, and for four sampling factors. In Fig. 4 the cross section was left constant as λ was varied. Instead, only a fraction, $1/\lambda$, of the possible scatterings were executed to account for the over-sampling. The lack of a sensitivity to λ suggests that the Boltzmann limit is reached even for $\lambda = 1$, i.e. n -body correlations do not significantly affect the flow. The same quantities were calculated in Fig. 5, except that the cross sections were scaled as $1/\lambda$ to account for the over-sampling. The results are then highly sensitive to λ which suggests that the finite interaction range that accompanies small λ leads to a reduced elliptic flow.

The reduction in longitudinal work and the damping of elliptic flow due to the incorporation of a finite-range interaction into a Boltzmann treatment suggests that viscous effects have effectively been introduced into the reaction.

IV. ANALYZING THE COLLISION KERNEL

In Sec. II B a finite range of interaction, characterized by a length scale, r , was shown to generate viscous behavior. This length scale is determined by the cross section, $r^2 \sim \sigma/\pi$, but the constant of proportionality is not trivially determined and can depend on seemingly arbitrary aspects of scattering algorithms. In the following subsection, we illustrate how viscous heating can also be directly related to the collision kernel by considering a simple example of one-dimensional expansion with a Bjorken space-time geometry. In the subsequent subsection we compare predictions based on the form of the scattering kernel with results from simulations based on the same kernel.

A. Viscous Heating in a Bjorken Expansion

As a simple example we again consider a one-dimensionally boost-invariant system of infinite extent in all dimensions. We keep the number of particles fixed so that the density scales inversely with τ ,

$$n(\tau) = \frac{1}{\tau} dN/(dA d\eta). \quad (30)$$

where the number of particles per area per rapidity interval, $dN/(dA d\eta)$, is fixed. To simplify matters we consider massless particles.

Here we wish to calculate the rate at which a particle at $\eta = 0$ has collisions with other particles, $dN_c/d\tau$, and the rate at which it gains or loses energy from such collisions, $d\langle E_1 \rangle/d\tau$. We assume the particles are in local thermal equilibrium, and analyze the collision kernel to determine the rates.

Referring to the colliding partners with the subscript ‘2’, the collision and heating rates per particle are

$$\frac{dN_c}{d\tau} = 2\pi \frac{dN}{dA d\eta} \int d\eta_2 r_2 dr_2 d^3 p_2 \frac{dN}{d^3 p_2} \cdot \delta(\tau_c - \tau) \Theta\left(\frac{\sigma}{\pi} - b^2\right), \quad (31)$$

$$\frac{d\langle E_1 \rangle}{d\tau} = 2\pi \frac{dN}{dA d\eta} \int d\eta_2 r_2 dr_2 d^3 p_2 \frac{dN}{d^3 p_2} \cdot \delta(\tau_c - \tau) \Theta\left(\frac{\sigma}{\pi} - b^2\right) \delta E_1. \quad (32)$$

Here, δE_1 is the average change in energy of the particle ‘1’ due to the collision and r_2 and η_2 describe the position of the second particle. The impact parameter for the two-particle collision is b and τ_c is the collision time.

The strategy employed here is to calculate the collision time, τ_c . The first particle is at a position $x_1 = (\tau, 0, 0, 0)$ with four momentum p_1 . The second particle is at a position $x_2 = (\tau \cosh \eta_2, r_2, 0, \tau \sinh \eta_2)$, with a four-momentum p_2 . Once τ_c is understood in terms of r_2 , η_2 , p_1 and p_2 , one can replace the delta function in the expression above,

$$\delta(\tau_c - \tau) \rightarrow \delta(r_c - r_2) \frac{\partial r_c}{\partial \tau_c}, \quad (33)$$

where r_c is the position required to make the collision occur at τ . By substituting the delta function with r_c for the delta function with τ_c , the integrals in Eq. (31) and Eq. (32) can be simplified and solved numerically.

The first step one must perform is to find τ_c in terms of r . The prescription for finding τ_c is somewhat arbitrary due to covariance issues. For our purposes, we will first define a time in the rest frame of the two particles where

the particles run abreast of one another, t_c . With $x_c = (t_c, 0, 0, 0)$ in the center-of-mass frame and $P = p_1 + p_2$, the collision time is determined by the condition,

$$(p_1 - p_2) \cdot (x'_1 - x'_2) = 0, \quad (34)$$

$$x'_1 = x_1 + \frac{P \cdot (x_c - x_1)}{P \cdot p_1} p_1, \quad (35)$$

$$x'_2 = x_2 + \frac{P \cdot (x_c - x_2)}{P \cdot p_2} p_2. \quad (36)$$

One can solve for $P \cdot x_c$,

$$P \cdot x_c = p_1 \cdot x_1 + p_2 \cdot x_2. \quad (37)$$

One can now solve for x'_1 and x'_2 .

$$x'_1 = x_1 + p_1 \frac{p_2 \cdot (x_2 - x_1)}{p_1 \cdot p_2} \quad (38)$$

$$x'_2 = x_2 + p_2 \frac{p_1 \cdot (x_1 - x_2)}{p_1 \cdot p_2} \quad (39)$$

If one calculated the times at which the collision occurred, t'_1 and t'_2 , they would only be simultaneous in the two-particle center-of-mass frame. Similarly, if one calculated $\tau'_1 = (t'^2_1 - z'^2_1)^{1/2}$ and $\tau'_2 = (t'^2_2 - z'^2_2)^{1/2}$, one would find that the two Bjorken proper times would not be simultaneous. One must arbitrarily choose a prescription to choose τ_c in terms of x'_1 and x'_2 . For our purposes, we choose the following prescription,

$$\tau_c^2 \equiv \frac{\tau'^2_1 + \tau'^2_2}{2} \quad (40)$$

Our only motivation in averaging the τ^2 s rather than the τ s is that the algebra simplified. Using this choice,

$$\tau_c^2 = \tau^2 + \frac{C_0 r'^2 + 2C_1 r' + C_2}{2} \quad (41)$$

$$C_0 = \gamma_1^2 p_{1\perp}^2 + \gamma_2^2 p_{2\perp}^2$$

$$C_1 = \gamma_1 \alpha_1 + \delta_1 \gamma_1 p_{1\perp}^2 + \gamma_2 \alpha_2 + \delta_2 \gamma_2 p_{2\perp}^2$$

$$C_2 = \delta_1^2 p_{1\perp}^2 + 2\delta_1 \alpha_1 + \delta_2^2 p_{2\perp}^2 + 2\delta_2 \alpha_2$$

The coefficients are defined

$$\alpha_1 = E_1 t - p_{1,z} z, \alpha_2 = E_2 t + p_{2,z} z \quad (42)$$

$$\delta_1 = 2z p_{2,z} / (p_1 \cdot p_2), \delta_2 = -2z p_{1,z} / (p_1 \cdot p_2)$$

$$\gamma_1 = 2p_{2,x} / (p_1 \cdot p_2), \gamma_2 = -2p_{1,x} / (p_1 \cdot p_2)$$

Here t , r and z are the positions describing the first particle in a frame where the particles are centered about $\eta = 0$ and $r = 0$.

$$\eta' = \frac{\eta_2}{2}, \quad t = \tau \cosh \eta', \quad z = -\tau \sinh \eta', \quad r' = \frac{r_2}{2}. \quad (43)$$

In terms of these new variables, one can rewrite the rates above,

$$\frac{dN_c}{d\tau} = 16\pi \frac{dN}{dA d\eta} \int d\eta' r' dr' d^3 p_2 \frac{dN}{d^3 p_2} \quad (44)$$

$$\cdot \delta(\tau - \tau_c) \Theta\left(\frac{\sigma}{\pi} - b^2\right)$$

$$= 16\pi \frac{dN}{dA d\eta} \int d\eta' r' dr' d^3 p_2 \frac{dN}{d^3 p_2}$$

$$\cdot \delta(r' - r_c) \frac{2\tau}{C_0 r' + C_1} \Theta\left(\frac{\sigma}{\pi} - b^2\right),$$

$$\frac{d\langle E_1 \rangle}{d\tau} = 16\pi \frac{dN}{dA d\eta} \int d\eta' r' dr' d^3 p_2 \frac{dN}{d^3 p_2} \quad (45)$$

$$\cdot \delta(r' - r_c) \frac{2\tau}{C_0 r' + C_1} \Theta\left(\frac{\sigma}{\pi} - b^2\right) \delta E_1.$$

When solving for r_c , there are two solutions to Eq. (41). If one uses solutions for both positive and negative r_c , the factor 16π should be reduced to 8π .

One can express these results as averages over p_1 and p_2

$$\frac{dN_c}{d\tau} = 32\pi\tau \frac{dN}{dA d\eta} \int d\eta' \left\langle \frac{r_c}{C_0 r_c + C_1} \right\rangle \cdot \Theta\left(\frac{\sigma}{\pi} - b^2\right), \quad (46)$$

$$\frac{d\langle E_1 \rangle}{d\tau} = 32\pi\tau \frac{dN}{dA d\eta} \int d\eta' \left\langle \frac{r_c}{C_0 r_c + C_1} \delta E_1 \right\rangle \Theta\left(\frac{\sigma}{\pi} - b^2\right). \quad (47)$$

If scattering angles are chosen with equal probability forwards and backwards, the average change in the two energies is

$$\delta E_1 = \frac{E_2 - E_1}{2}. \quad (48)$$

The non-local aspect of the collision kernel should contribute to heating the particles in their local frame. From physical arguments, one expects the non-local contribution to heating to scale with temperature, density, time and cross section in a simple manner.

$$\begin{aligned} \frac{dE_\perp}{d\tau} &= \frac{3}{4\pi} \frac{d\langle E_1 \rangle}{d\tau} \\ &= \beta \frac{dN}{dA d\eta} \frac{\sigma^2 T}{\tau^3}, \end{aligned} \quad (49)$$

where E_t is the mean transverse energy per particle and β is a dimensionless constant.

The simple scaling derives from the hydrodynamically motivated Eq.s (12) and (13). One expects the collision rate to scale proportional to the density, which requires the factor $dN/(dA d\eta)$ and one inverse power of τ , and the cross-section. The squared-velocity gradient suggests an extra factor of τ^{-2} , and the range of the interaction requires an extra factor of σ . The constant β is determined by the form of the differential cross section, e.g., s -wave scattering would result in a higher β than a highly forward-peaked form. Since one power of σ comes from the range of interaction, β should scale inversely with the sampling factor λ . Finally, the effective mass should be proportional to the temperature.

The heating rate due to non-local interactions is calculated from Eq. (47) by numerically analyzing the collision kernel and is displayed in Fig. 6 after being scaled by the temperature, time and cross section. Had the simple scaling argument been correct the ratio would have been a constant β . However, due to higher order corrections in $1/\tau$, the ratio varies as a function of τ . The ratio approaches a constant for large τ , $\tau^2 \gg \sigma$. The scaling fails when τ becomes less than the range of the interaction, which for this example is ~ 1.0 fm due to the 10 mb cross section. The departure of the ratio from a straight line illustrates the limitation of simple hydrodynamic arguments to describe the viscous heating from non-local interactions.

B. Comparing to Numerical Results

Finally, we present numerical results involving a boost-invariant Boltzmann description (GROMIT- τ) which was executed with cyclic boundary conditions, both in η and in the transverse coordinates. We compare the viscous heating rate observed in the numerical calculation with the viscous heating rate expected from the scaling arguments expressed in Eq. (49), where the coefficient β was determined from analyzing the collision kernel from the last section. The temperature was set to 400 MeV at a time $\tau = 0.1$ fm/c, and the cross section was chosen to be 10 mb. A simple s -wave form was used for the angular dependence of the cross section.

The resulting mean transverse energy is displayed in Fig. 7 as a function of τ . The initial heating derives from the non-local nature of the interactions. Longitudinal cooling ultimately dominates the behavior as the non-local contribution to the heating falls roughly at τ^{-3} .

The dotted line in Fig. 7 describes the evolution of the transverse energy in the limit of ideal (non-viscous) hydrodynamics. In that limit, the stress-energy tensor has a simple form,

$$T^{\alpha\beta} = \epsilon u^\alpha u^\beta + P(u^\alpha u^\beta - g^{\alpha\beta}). \quad (50)$$

In the Bjorken limit, $\partial v/\partial z = 1/\tau$ and the evolution of the energy density becomes

$$\frac{\partial}{\partial t}\epsilon = -\frac{P + \epsilon}{\tau}. \quad (51)$$

For the massless case, $P = \epsilon/3$, which gives the result,

$$\epsilon(\tau) = \epsilon(\tau_0) \left(\frac{\tau}{\tau_0}\right)^{-4/3} \quad (52)$$

The velocity gradient generates a shear which contributes an additional term to the stress-energy tensor.

$$T_\eta^{\alpha\beta} = \eta(-g^{\alpha\gamma} - u^\alpha u^\gamma) \left(\frac{\partial u_\gamma}{\partial x_\beta} + \frac{\partial u_\beta}{\partial x_\gamma} - \frac{2}{3} g_\gamma^\beta \partial \cdot u \right). \quad (53)$$

In a simulation, one can determine η_{NS} by evaluating the stress-energy tensor.

$$\frac{T^{xx} + T^{yy}}{2} - T^{zz} = 2\frac{\eta_{NS}}{\tau}. \quad (54)$$

The components of the stress-energy tensor are extracted by analyzing the momenta of particles as measured in the local rest frame.

$$T_{ij} = \frac{1}{V} \sum \frac{p_i p_j}{E_p}. \quad (55)$$

The Navier-Stokes evolution of the energy density is governed by the equation,

$$\frac{\partial}{\partial \tau}\epsilon = -\frac{P + \epsilon}{\tau} + \frac{4}{3} \frac{\eta_{NS}}{\tau^2}. \quad (56)$$

For massless particles interacting with a constant cross section, dimensional arguments force the viscosity to rise linearly with τ since the mean free path should grow with τ due to the density falling as $1/\tau$.

$$\eta_{NS} = C_{NS}\epsilon\tau, \quad (57)$$

where C_{NS} is a constant, determined only by the form of the cross section. The energy density then follows the Navier Stokes form [21]. This form should be valid unless the viscous contribution to the stress energy tensor approaches the same order as the equilibrated pressure [22].

$$\epsilon(\tau) = \epsilon(\tau_0) \left(\frac{\tau}{\tau_0}\right)^{-(4/3)(1-C_{NS})}. \quad (58)$$

The Navier Stokes result is represented by a dashed line in Fig. 7. The value of C_{NS} was determined by evaluating the asymmetry of the stress-energy tensor in the simulation at large times. Running simulations with a large sampling ratios generated results in excellent agreement with the Navier Stokes result.

The inclusion of non-local effects is responsible for the discrepancy between the simulation results in Fig. 7 and the Navier-Stokes results. Eq. (13) suggests that the non-local correction to the viscosity should scale proportional to τ^{-2} ,

$$\eta_{nl} = C_{nl}\epsilon/\tau, \quad (59)$$

where C_{nl} is independent of τ and scales with σ^2 as explained in the previous section. One can now determine the evolution of the energy density by solving the hydrodynamical equations of motion,

$$\frac{\partial}{\partial \tau}\epsilon = -\frac{4}{3}(1 - C_{NS})\frac{\epsilon}{\tau} + \frac{4}{3}C_{nl}\frac{\epsilon}{\tau^3} \quad (60)$$

$$(61)$$

This equation has a simple solution.

$$\epsilon(\tau) = \epsilon(\tau_0) \left(\frac{\tau}{\tau_0} \right)^{4/3(1-C_{NS})} \exp \left\{ \frac{2C_{nl}}{3} \left(\frac{1}{\tau_0^2} - \frac{1}{\tau^2} \right) \right\}. \quad (62)$$

This form is shown with the solid lines in Fig. 7. The constant C_{nl} was determined by the asymptotic limit of Fig. 6. The effect of non-local interactions is somewhat overestimated at small times by Eq. (62) as would be expected by considering Fig. 6 which shows that that growth of the viscous heating at small τ is somewhat slower than the naive expectation that it scales as τ^{-3} .

The effect of non-local interactions is lessened for scatterings that are more forward peaked. Fig. 8 illustrates the behavior of E_t as a function of τ for a screened Rutherford scattering,

$$\frac{d\sigma}{dt} = \frac{9\pi}{2} \frac{\alpha_s^2}{(t - \mu^2)^2}, \quad (63)$$

$$\sigma = \frac{9\pi\alpha_s^2}{2\mu^2}, \quad (64)$$

$$t = (p_1 - p_3)^2. \quad (65)$$

Here, $\alpha_s = \sqrt{2/9}$, and the screening mass μ is chosen to provide a cross section of 10 mb. As compared to the s -wave scattering result in Fig. 7, the effect of non-local interactions is diminished while the Navier-Stokes viscosity is increased. This is expected since the mean free path is effectively increased while the energy transfer inherent to collisions is decreased.

V. DISCUSSION AND SUMMARY

The effects of short-range, but non-local, interactions provide an unwelcome complication to the analysis and interpretation of experimental results from relativistic heavy ion collisions. Flow observables are most significantly affected, especially elliptic flow. Thus, the additional length scale, characteristic of hard collisions, interferes with our ability to extract bulk matter properties due to the finite volume in space-time subtended by heavy ion collisions.

By increasing the sampling ratio in Boltzmann treatments while simultaneously reducing the cross section, one can effectively eliminate these effects in models. Aside from simplifying the analysis, large sampling ratios are attractive as they eliminate sensitivities to a variety of arbitrary choices inherent to simulations and solve a variety of problems related to acausal propagation. However, in nature particles indeed interact over a finite range, either by exchange of off-shell particles or through a mutual interaction through classical fields. Therefore, it is important to understand the degree to which these effects are physical as opposed to representing numeric artifacts.

Determining the correct range for non-local interactions in the first fm/c of a collision might require correctly taking into account both relativity and quantum effects. For instance, one might determine the extent by considering the transfer of momentum and energy through exchange of off-shell particles in the context of a Wigner decomposition of the propagator [4]. This object might then be analyzed in a manner analogous to the method in which the classical scattering kernel was studied in Sec. IV. However, this is beyond the scope of the current paper.

On the optimistic side, non-local effects can be interpreted in terms of viscous parameters as shown in Sec. II B. This allows the incorporation of non-local effects into hydrodynamic codes in a straight-forward manner. Knowing the viscous parameters would also provide criteria for tuning Boltzmann algorithms so that they are consistent with quantum transport considerations. The tuning could be accomplished by changing either the sampling factor or by adjusting scattering algorithms. The simple manner with which the viscous parameters scale with density and cross-section should simplify such a procedure.

As transport theories address the first one fm/c of a relativistic heavy ion collision, the role of non-local interactions becomes increasingly important. For times above 2 fm/c, it is unlikely that the non-localities play any significant role as the effects scale as τ^{-3} . Since the nuclei pass one another at RHIC in less than 0.2 fm/c, whereas cross sections might approach a square fm, non-local effects might provide a non-negligible source of stopping as the viscous drag converts longitudinal collective velocity to heat. The role for such effects in the stopping phase at LHC collisions should be even greater.

Finally, we mention the effect of non-local interactions one might expect in the earliest moments of the big bang. In that case cross sections should become perturbative and particles should be approximately massless. In this case cross sections should scale as α^2/T^2 , where α is the unified coupling constant. Since T would scale as $1/\tau$, the Navier-Stokes viscosity and the non-local viscosity should both scale identically with τ . Since the non-local terms scale as σ^2 while the Navier-Stokes terms scale as σ^{-1} , the terms would differ in importance by a constant proportional to α^6 . Thus, if the system becomes perturbative, one expects the non-local terms to be negligible compared to the

Navier-Stokes terms. However, the physics of high-energy hadronic collisions is far from perturbative, and the large coupling constants magnify the importance of the non-local terms relative to Navier-Stokes terms.

ACKNOWLEDGMENTS

This work was supported by the National Science Foundation, grant PHY-00-70818, and by the Department of Energy under Contract No. DE-AC02-98CH10886 and Contract No. DE-FG-02-93ER-10761. B. Zhang's work was partly supported by the Arkansas Science and Technology Authority Grant No. 01-B-20.

- [1] S. Weinberg, *Gravitation and Cosmology*, John Wiley & Sons, p. 55 (1972).
- [2] C.-Y. Wong, *Phys. Rev. C***25**, 1460 (1982).
- [3] G.F. Bertsch, H. Kruse and S. Das Gupta, *Phys. Rev. C***29**, 673 (1984).
- [4] D.A. Brown and P. Danielewicz, *Phys. Rev. D***58**, 094003 (1998).
- [5] D.E. Kahana, D. Keane, Y. Pang, T. Schlagel and S. Wang, *Phys. Rev. Lett.* **74**, 4404 (1995).
- [6] P. Danielewicz and S. Pratt, *Phys. Rev. C***53**, 249 (1996).
- [7] G. Kortemeyer, W. Bauer, K. Haglin, G. Kortemeyer and S. Pratt, *Phys. Rev. C***52**, 2714 (1995).
- [8] B. Zhang and Y. Pang, *Phys. Rev. C***56**, 2185 (1997).
- [9] B. Zhang, *Comput. Phys. Commun.* **109**, 193 (1998).
- [10] RHIC Transport Theory Collaboration, <http://www.nscl.msu.edu/~rttc>.
- [11] D. Molnár and M. Gyulassy, *Phys. Rev. C***62**, 054907 (2000).
- [12] J.D. Bjorken, *Phys. Rev. D***27**, 1327 (1983).
- [13] D. Molnár and M. Gyulassy, LANL report nucl-th/0104073 (2001).
- [14] J.-Y. Ollitrault, *Nucl. Phys. A***638**, 195c (1998).
- [15] P. Danielewicz, *Nucl. Phys. A***673**, 375 (2000).
- [16] C. Pinkenburg, et al., *Phys. Rev. Lett.* **83**, 1295 (1999).
- [17] A.M. Poskanzer et al., *Nucl. Phys. A***661**, 344 (1999).
- [18] H. Sorge, *Phys. Rev. Lett.* **82**, 2049 (1999).
- [19] B. Zhang, M. Gyulassy and C.M. Ko, *Phys. Lett. B***455**, 45 (1999).
- [20] K.H. Ackermann et al., *Phys. Rev. Lett.* **86**, 402 (2001).
- [21] M. Gyulassy, Y. Pang and B. Zhang, *Nucl. Phys. A***626**, 999 (1997);
- [22] P. Danielewicz and M. Gyulassy, *Phys. Rev. D***31**, 53 (1985).

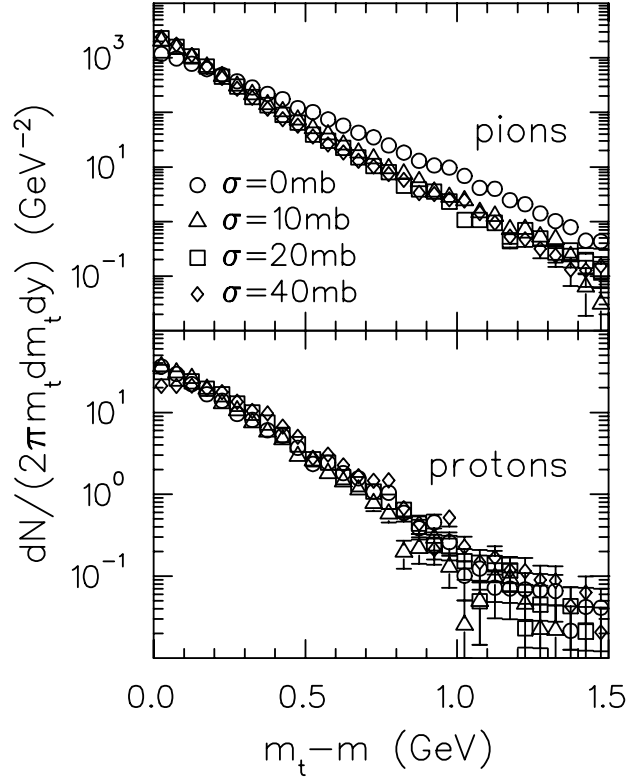


FIG. 1. Spectra from GROMIT- τ are displayed for four cross sections.

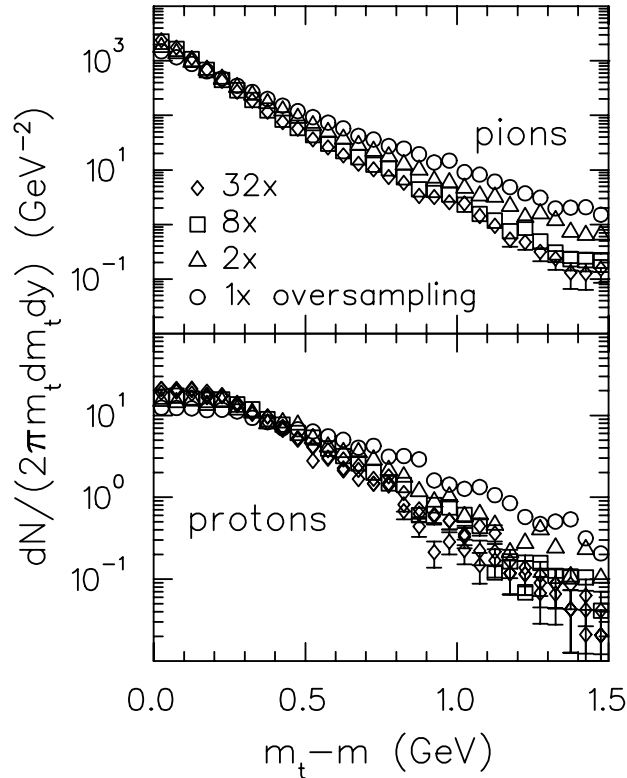


FIG. 2. Spectra for pions and protons resulting from GROMIT- τ with 40 mb cross sections for four sampling factors, $\lambda = 1, 2, 8, 32$.

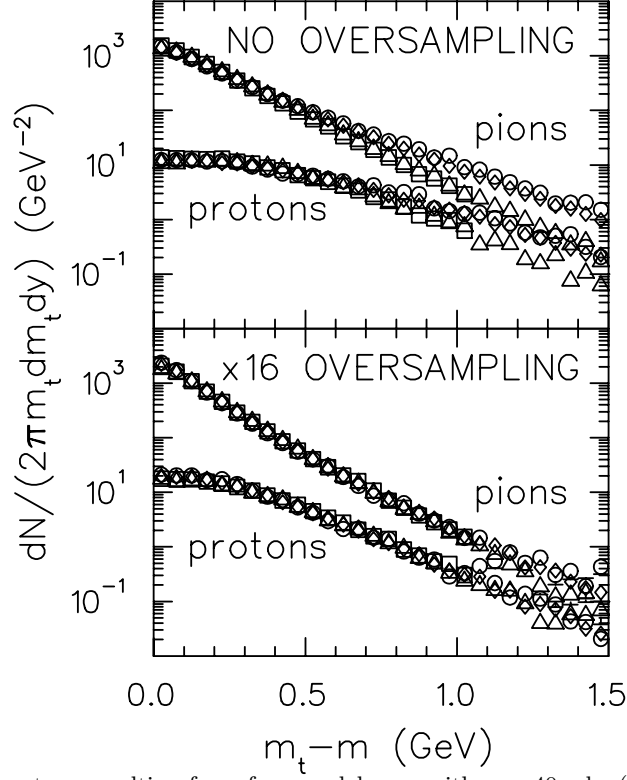


FIG. 3. Spectra for pions and protons resulting from four models run with $\sigma = 40$ mb: (ZPC – squares, MPC – diamonds, GROMIT-t – triangles, GROMIT- τ – circles). In the upper panel calculations were performed with a sampling factor of 1, while in the lower panel each model used a sampling factor $\lambda = 16$. Due to different scattering algorithms, the models generated different results for $\lambda = 1$, while generating identical results for larger λ .

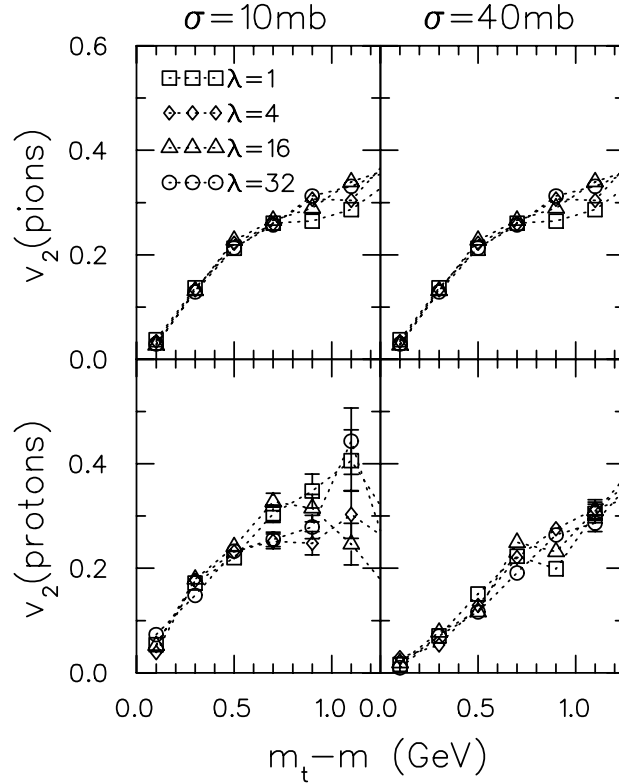


FIG. 4. Elliptic flow is shown as a function of transverse energy for both pions and protons for several sampling factors, λ . The cross sections were not varied as λ was varied, but instead only a fraction $1/\lambda$ of the particles were scattered. The insensitivity to λ demonstrates that the Boltzmann limit is effectively realized, even for $\lambda = 1$.

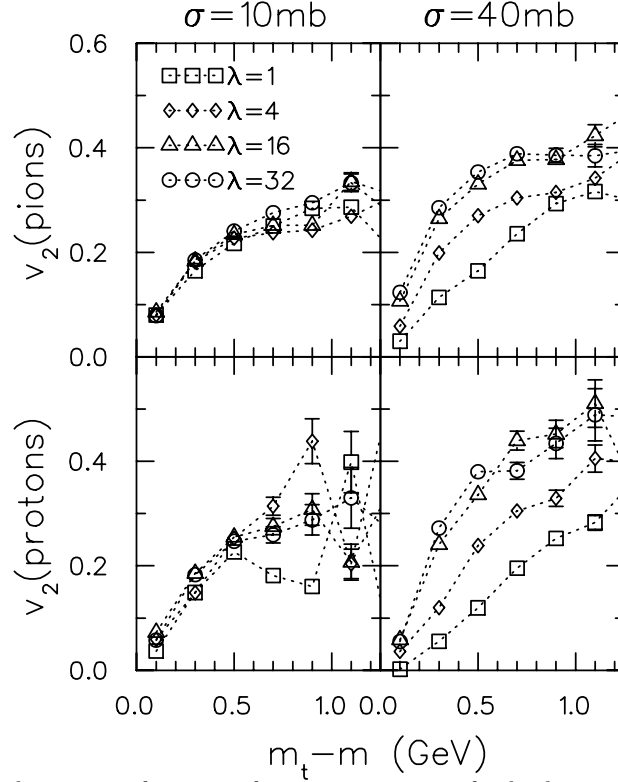


FIG. 5. Again, elliptic flow is shown as a function of transverse energy for both pions and protons for several sampling factors. In this case the cross sections were scaled by a factor $1/\lambda$ to account for the over-sampling. The reduced flow resulting for calculations with small λ (larger cross sections) is attributed to viscous effects arising from the finite interaction range.

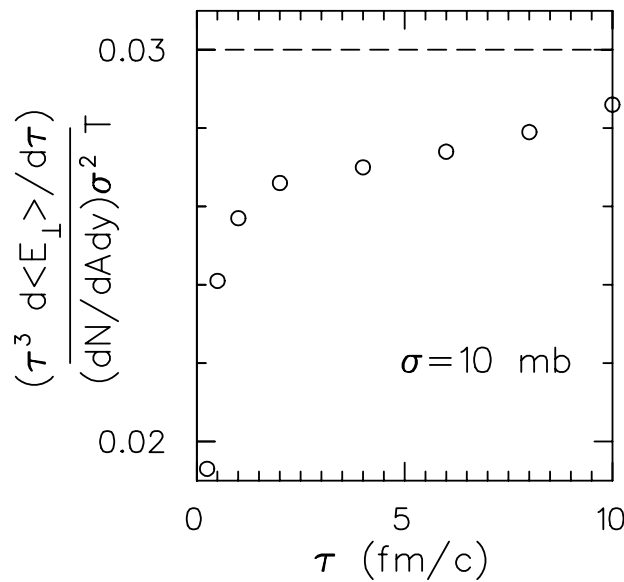


FIG. 6. The heating due to non-local interactions as calculated numerically from the collision kernel (circles) is scaled in such a way that it would be constant if the simple hydrodynamic scaling arguments were valid. The dashed line represents the asymptotic value.

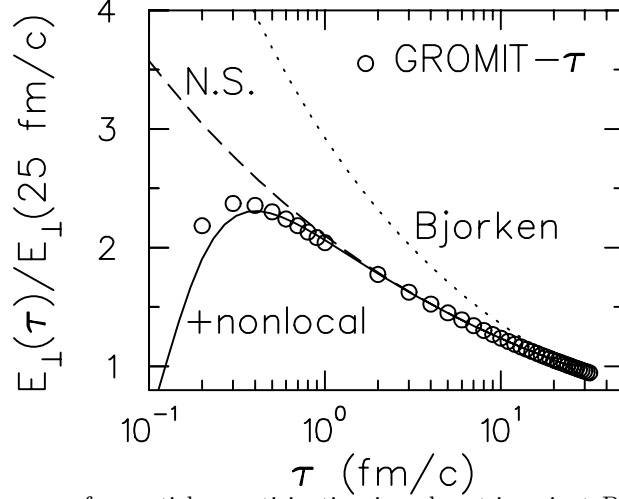


FIG. 7. The mean transverse energy for particles participating in a boost-invariant Bjorken expansion is displayed as a function of the proper time (circles). Also displayed are the Bjorken hydrodynamic result (dotted line), the Navier-Stokes correction which accounts for viscous shear arising from a finite mean free path (dashed line) and the correction due to non-local interactions as expected from simple scaling arguments (solid line). Non-local interactions are important at small times when the velocity gradients and collision rates are high.

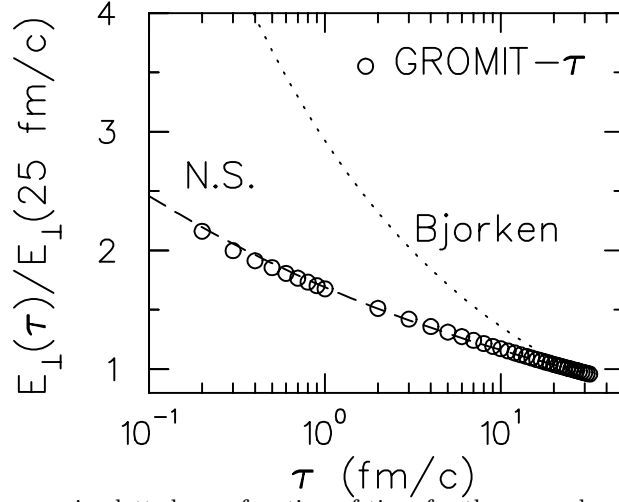


FIG. 8. The mean transverse energy is plotted as a function of time for the case where a forward-peaked cross section as described in Eq. (63) is implemented. The results from GROMIT- τ (circles) are well described by the Navier-Stokes (dashed line) correction to the Bjorken solution (dotted line). As compared to s -wave scattering, the Navier-Stokes viscosity is increased while the non-local contribution to the viscosity becomes negligible.